

Supplementary Materials

Table of Contents

Supplementary Table 1: Variants associated with waist-to-hip ratio adjusted for body mass index (WHR_{adjBMI}) in the discovery genome-wide analysis of rare non-synonymous variants.	1
Supplementary Table 2. a. Correlation between the UK Biobank WES data and the genotype data for rare nonsynonymous variants with a minor allele frequency (MAF) between 0.1% - 0.5% in overlapping samples. b. Box plot of rare allele concordance between the UK Biobank WES data and the genotype data for rare nonsynonymous variants with a MAF between 0.1% - 0.5% in overlapping samples.	2
Supplementary Table 3: a. Conditionally independent index variants and fine-mapping at the <i>CALCRL</i> , <i>PLIN1</i> , <i>PDE3B</i> and <i>ACVR1C</i> loci. b. Formal conditional analyses at the <i>CALCRL</i> , <i>PLIN1</i> , <i>PDE3B</i> and <i>ACVR1C</i> loci.	3
Supplementary Table 4: Conditionally-independent index variants at the <i>ABHD15</i> , <i>PYGM</i> , <i>PLCB3</i> and <i>FNIP1</i> regions.	5
Supplementary Table 5: STAAR-O (2) gene-based results for genes discovered in the single variant analysis.	6
Supplementary Table 6: Significant gene-based results from the exome-wide scan for WHR_{adjBMI}	7
Supplementary Table 7: Sex-specific results for gene-based analysis.	8
Supplementary Table 8: Quality control measurements for variants included in the refined gene-based tests and single marker association results for all included variants.	9
Supplementary Table 9: a. Summary statistics for quantitative traits from gene-based association analyses in sex-combined, women-only and male-only data. b. Summary statistics for binary traits from gene-based association analyses in sex-combined, women-only and male-only data. Details for all phenotypes and are given on Supplementary Table 12.	9
Supplementary Table 10: a. Lookup from Type 2 Diabetes Knowledge Portal for type 2 diabetes.	10
Supplementary Table 11: Leave one out analysis results for the most significant single variant in significant genes.	14
Supplementary Table 12. Phenotypes used for phenotypic associations in UK Biobank.	15
Supplementary Figure 1: Regional association plots of the overall and statistically-decomposed signals at the <i>CALCRL</i> , <i>PLIN1</i> , <i>PDE3B</i> and <i>ACVR1C</i> genes.	17
Supplementary Figure 2: Association of the significant genes with other body fat distribution or cardiometabolic trait related phenotypes in UK Biobank for (a) continuous phenotypes and (b) binary phenotypes. There was no rare predicted loss of function variant carriers for <i>INSR</i> in coronary heart disease (CHD) cases in women-only analyses. Abbreviations: pLoF, predicted loss of function; WHR_{adjBMI} ; waist-to-hip ratio adjusted for body mass index; BMI, body mass index; TG, triglycerides; HD; high density lipoprotein, LDL low-density lipoprotein; TG/HDL, triglyceride to high density lipoprotein ratio; T2D, type 2 diabetes; CHD, coronary heart disease.	18

Supplementary Note 1: Genomic context analyses at the <i>PLIN1</i> , <i>ACVR1C</i> , <i>PDE3B</i> and <i>CALCRL</i> loci.	20
Supplementary Note 2: Genomic context analyses at the <i>ABHD15</i> , <i>PYGM</i> , <i>PLCB3</i> and <i>FNIP1</i> loci.	21
Supplementary Note 3: Predictions regarding the variants identified through single marker analysis.	22
REFERENCES	26

Supplementary Table 1: Variants associated with waist-to-hip ratio adjusted for body mass index (WHR_{adjBMI}) in the discovery genome-wide analysis of rare non-synonymous variants.

Gene	dbSNP rsID	Genomic coordinate, chromosome and position	Effect allele and other allele	Effect allele frequency in % (minor allele count)	Protein change (amino acid corresponding to the effect allele)	Beta (SE) for WHR _{adjBMI} per effect allele in univariate analysis, in SD units	p-value	Beta (SE) for WHR _{adjBMI} per effect allele in conditional analyses*, in SD units	p-value conditional analyses*
<i>Sex-combined</i>									
<i>PLIN1</i>	rs139271800	chr15:89671546	G and A	0.1 (1,127)	p.L90P (P)	-0.21 (0.029)	5.5×10 ⁻¹³	-0.21 (0.029)	5.5×10 ⁻¹³
<i>PDE3B</i>	rs150090666	chr11:14843853	T and C	0.1 (932)	p.R783X (X)	-0.26 (0.032)	1.4×10 ⁻¹⁵	-0.25 (0.032)	6.2×10 ⁻¹⁵
<i>ACVR1C</i>	rs56188432	chr2:157550353	G and A	0.2 (2,113)	p.I195T (T)	-0.14 (0.021)	4.9×10 ⁻¹¹	-0.14 (0.021)	5.4×10 ⁻¹²
<i>CALCLRL</i>	rs61739909	chr2:187380712	G and A	0.3 (2,954)	p.L87P (P)	-0.13 (0.018)	2.0×10 ⁻¹³	-0.12 (0.018)	5.9×10 ⁻¹²
<i>ABHD15</i>	rs141385558	chr17:29566527	T and C	0.3 (2,441)	p.G147D (D)	0.11 (0.019)	6.3×10 ⁻⁹	0.07 (0.019)	0.00019
<i>PYGM</i>	rs116987552	chr11:64759751	A and G	0.4 (3,764)	p.R50X (X)	0.09 (0.016)	7.0×10 ⁻⁹	0.06 (0.015)	0.00037
<i>Sex-specific analysis in women ‡</i>									
<i>PLCB3</i>	rs145502455	chr11:64263558	A and G	0.4 (2,028)	p.V806I (I)	0.13 (0.021)	1.6×10 ⁻¹⁰	0.03 (0.020)	0.11
<i>FNIP1</i>	rs115209326	chr5:131672891	T and C	0.3 (1,655)	p.R518Q (Q)	-0.13 (0.023)	4.8×10 ⁻⁹	-0.12 (0.023)	3.8×10 ⁻⁷

Analyses are from 450,562 European ancestry individuals. Genomic coordinates according to human genome reference sequence hg38.

* Adjusting for conditionally-independent index variants highlighted in the joint conditional model (see Supplementary Table 3 for list of index variants at loci where fine-mapping supported causal role of these variants and Supplementary Table 4 for other loci).

‡ Variants in addition to the one of the sex-combined primary analysis which were identified in a secondary analysis in 244,478 women from the UK Biobank study ($p < 5 \times 10^{-8}$).

Abbreviations: SE, standard error; WHR, waist-to-hip ratio; BMI, body mass index; SD, standard deviation.

Supplementary Table 2. a. Correlation between the UK Biobank WES data and the genotype data for rare nonsynonymous variants with a minor allele frequency (MAF) between 0.1% - 0.5% in overlapping samples. b. Box plot of rare allele concordance between the UK Biobank WES data and the genotype data for rare nonsynonymous variants with a MAF between 0.1% - 0.5% in overlapping samples.

a.

Min	1 st Q	Median	Mean	3 rd Q	Max
0.002	0.989	0.996	0.988	0.999	1

b.

Min	1 st Q	Median	Mean	3 rd Q	Max
0.002	0.991	0.997	0.987	0.999	1

Supplementary Table 3: a. Conditionally independent index variants and fine-mapping at the *CALCRL*, *PLINI*, *PDE3B* and *ACVR1C* loci.

Analyses are from 450,562 European ancestry individuals. Beta and standard errors are in standardized units of BMI-adjusted WHR per copy of the effect allele. Genomic coordinates according to human genome reference sequence GRCh38. **b. Formal conditional analyses at the *CALCRL*, *PLINI*, *PDE3B* and *ACVR1C* loci.** Formal conditional analyses were conducted using individual-level genotype data in a subset of 350,721 unrelated European ancestry participants of UK Biobank. Because this is a subset of the discovery study, associations estimates differ from those presented in Supplementary Table 1.

a.

Locus	Signal	dbSNP rsID	Genomic coordinate, chromosome, position, effect allele, other allele (effect allele frequency, %)	Annotation	Beta (SE) from univariate analysis, in SD units	p-value univariate analysis	Beta (SE) from conditional analysis*, in SD units	p-value conditional analysis*	Genomic position of 99% credible set window, (width in number of base pairs)	Number of variants in the credible set	PPA for the index variant, %
<i>PLINI</i>	1‡	rs139271800	chr15:89671546:G:A (0.1%)	<i>PLINI</i> p.L90P	-0.21 (0.029)	5.5×10 ⁻¹³	-0.21 (0.029)	5.5×10 ⁻¹³	89671546 (1)	1	>99%
<i>PDE3B</i>	1‡	rs150090666	chr11:14843853:T:C (0.1%)	<i>PDE3B</i> p.R783X	-0.26 (0.032)	1.4×10 ⁻¹⁵	-0.25 (0.032)	6.2×10 ⁻¹⁵	14843853 (1)	1	>99%
	2	rs2970332	chr11:14338889:G:A (23.1%)	<i>RRAS2</i> intronic	-0.02 (0.002)	9.9×10 ⁻¹²	-0.02 (0.002)	6.3×10 ⁻¹²	14236464-14667794 (431,331)	20	23%
	3	rs79634051	chr11:14540399:C:G (2.8%)	<i>PSMA1</i> intronic	-0.03 (0.006)	6.4×10 ⁻⁸	-0.04 (0.006)	2.1×10 ⁻⁹	14221316-14869595 (648,280)	15	78%
<i>ACVR1C</i>	1	rs55920843	chr2:157556189:G:T (1.2%)	<i>ACVR1C</i> p.N150H	-0.08 (0.009)	8.9×10 ⁻¹⁹	-0.09 (0.009)	4.6×10 ⁻²⁰	157556189 (1)	1	>99%
	2	rs2444770	chr2:157647227:C:T (14.8%)	18kb 5' of <i>ACVR1C</i>	-0.02 (0.003)	5.9×10 ⁻¹³	-0.02 (0.003)	7.7×10 ⁻¹⁵	157639990-157661726 (21,737)	7	46%
	3‡	rs56188432	chr2:157550353:G:A (0.2%)	<i>ACVR1C</i> p.I195T	-0.14 (0.021)	4.9×10 ⁻¹¹	-0.14 (0.021)	5.4×10 ⁻¹²	157550353 (1)	1	>99%
<i>CALCRL</i>	1	rs10177093	chr2:187349092:G:T (45.6%)	<i>CALCRL</i> intronic	-0.02 (0.002)	2.2×10 ⁻²⁷	-0.02 (0.002)	7.7×10 ⁻²⁶	187223800-187349092 (125,293)	60	17%
	2‡	rs61739909	chr2:187380712:G:A (0.3%)	<i>CALCRL</i> p.L87P	-0.13 (0.018)	2.0×10 ⁻¹³	-0.12 (0.018)	5.9×10 ⁻¹²	187380712-187405532 (24,821)	2	51%

* Adjusting for conditionally-independent index variants highlighted in the joint conditional model.

‡ Variant identified in the genome-wide scan of rare nonsynonymous variants.

Abbreviations: SE, standard error; SD, standard deviation; PPA, posterior probability of association.

b.

Locus	Signal number	dbSNP rsID	Beta (SE) from univariate analysis	p-value univariate analysis	Beta (SE) from conditional analyses	p-value conditional analyses
<i>CALCRL</i>	1	rs10177093	-0.02 (0.002)	4.4×10^{-22}	-0.02 (0.002)	2.2×10^{-20}
	2	rs61739909	-0.15 (0.021)	9.8×10^{-13}	-0.14 (0.021)	5.5×10^{-11}
<i>PLINI</i>	1	rs139271800	-0.16 (0.034)	2.3×10^{-6}	-0.16 (0.034)	2.3×10^{-6}
<i>PDE3B</i>	1	rs150090666	-0.24 (0.037)	2.0×10^{-11}	-0.24 (0.037)	1.7×10^{-10}
	2	rs2970332	-0.02 (0.003)	9.8×10^{-8}	-0.02 (0.003)	1.2×10^{-7}
	3	rs79634051	-0.03 (0.007)	2.9×10^{-5}	-0.03 (0.007)	2.0×10^{-6}
<i>ACVR1C</i>	1	rs55920843	-0.09 (0.011)	3.1×10^{-15}	-0.09 (0.011)	3.0×10^{-16}
	2	rs2444770	-0.02 (0.003)	2.8×10^{-10}	-0.02 (0.003)	1.7×10^{-11}
	3	rs56188432	-0.14 (0.025)	9.9×10^{-9}	-0.15 (0.025)	4.7×10^{-9}

Supplementary Table 4: Conditionally-independent index variants at the *ABHD15*, *PYGM*, *PLCB3* and *FNIP1* regions.

Locus	dbSNP rsID	Chromosome and position
<i>Sex-combined</i>		
<i>ABHD15</i>	rs62070804	17: 29562625
<i>ABHD15</i>	rs561089333	17: 30422242
<i>PYGM</i>	rs224170	11: 63897410
<i>PYGM</i>	rs12419038	11: 64145264
<i>PYGM</i>	rs3751122	11: 64185649
<i>PYGM</i>	rs11231721	11: 64190363
<i>PYGM</i>	rs7952318	11: 64193770
<i>PYGM</i>	rs56271783	11: 64237251
<i>PYGM</i>	rs75152214	11: 64543641
<i>PYGM</i>	rs186402106	11: 64700853
<i>PYGM</i>	rs2306363	11: 65638129
<i>PYGM</i>	rs10750766	11: 65706327
<i>PYGM</i>	rs4645917	11: 65714169
<i>PYGM</i>	rs593982	11: 65745636
<i>Sex-specific analysis in women †</i>		
<i>PLCB3</i>	rs11231698	11: 64109691
<i>PLCB3</i>	rs3751122	11: 64185649
<i>PLCB3</i>	rs138055838	11: 64220169
<i>PLCB3</i>	rs56271783	11: 64237251
<i>PLCB3</i>	rs186826945	11: 64452647
<i>FNIP1</i>	rs74667082	5: 131412611

Conditional analyses estimated the association of each index variant while adjusting for all other index variants at the region. Index variants were selected using a joint meta-analysis model with GCTA (1).

† Identified in a secondary analysis in 244,478 women from the UK Biobank study ($p < 5 \times 10^{-8}$).

Supplementary Table 5: STAAR-O (2) gene-based results for genes discovered in the single variant analysis.

Category	Gene	Number of Variants	Pval	Beta	SE
pLoF	<i>PLIN1</i>	31	9.82×10^{-9}	-0.27	0.05
Moderate	<i>PLIN1</i>	216	9.21×10^{-6}	-0.02	0.01
pLoF + Moderate	<i>PLIN1</i>	292	4.94×10^{-6}	-0.03	0.01
pLoF	<i>ACVR1C</i>	9	5.50×10^{-2}	-0.48	0.24
Moderate	<i>ACVR1C</i>	130	4.57×10^{-7}	-0.15	0.03
pLoF + Moderate	<i>ACVR1C</i>	139	1.68×10^{-7}	-0.15	0.03
pLoF	<i>PDE3B</i>	65	1.41×10^{-6}	-0.21	0.04
Moderate	<i>PDE3B</i>	392	8.12×10^{-2}	-0.007	0.01
pLoF + Moderate	<i>PDE3B</i>	437	2.26×10^{-5}	-0.03	0.01
pLoF	<i>CALCRL</i>	19	1.10×10^{-1}	0.31	0.14
Moderate	<i>CALCRL</i>	114	1.12×10^{-3}	-0.07	0.02
pLoF + Moderate	<i>CALCRL</i>	133	1.16×10^{-3}	-0.06	0.02

Abbreviations: pLOF, predicted loss of function; Pval, STAAR-O p-value; Beta, effect size; SE, standard error.

Supplementary Table 6: Significant gene-based results from the exome-wide scan for WHR_{adjBMI} .

Category	Gene	Number of variants	Genotype counts (RR/RA/AA)	Pval	Beta	SE
pLoF	<i>PLIN4</i>	65	183,900/1,065/0	5.86×10^{-7}	0.16	0.03
pLoF	<i>PLIN1</i>	31	184,572/388/5	9.82×10^{-9}	-0.27	0.05
pLoF	<i>INSR</i>	27	184,904/61/0	6.21×10^{-7}	-0.64	0.12
Moderate	<i>ACVR1C</i>	130	183,551/1,414/0	4.57×10^{-7}	-0.15	0.03
pLoF + Moderate	<i>ACVR1C</i>	139	183,535/1,430/0	1.68×10^{-7}	-0.15	0.03
pLoF	<i>PDE3B</i>	44	184,474/491/0	1.41×10^{-6}	-0.21	0.04

Abbreviations: pLOF, predicted loss of function; MAF, minor allele frequency; Pval, STAAR-O p-value; Beta, effect size; SE, standard error; RR, reference/reference genotype; RA, reference/alternate genotypes; AA, alternate/alternate genotypes.

Supplementary Table 7: Sex-specific results for gene-based analysis.

Gene			Women (n=101,569)			Men (n=82,677)		
Category	Gene	P_sexdiff	Beta	SE	Pval	Beta	SE	Pval
pLoF	<i>PLIN4</i>	2.08×10^{-2}	0.214	0.039	1.66×10^{-7}	0.073	0.046	1.55×10^{-1}
pLoF	<i>PLIN1</i>	2.83×10^{-1}	-0.330	0.065	8.96×10^{-8}	-0.223	0.075	4.56×10^{-3}
pLoF	<i>INSR</i>	4.62×10^{-7}	-1.218	0.168	1.44×10^{-12}	0.046	0.186	7.53×10^{-1}
Moderate	<i>ACVR1C</i>	1.13×10^{-1}	-0.181	0.035	7.78×10^{-7}	-0.098	0.039	5.28×10^{-2}
pLoF + Moderate	<i>ACVR1C</i>	1.22×10^{-1}	-0.183	0.034	4.60×10^{-7}	-0.103	0.039	4.03×10^{-2}
pLoF	<i>PDE3B</i>	1.85×10^{-3}	-0.334	0.059	5.04×10^{-8}	-0.057	0.067	1.87×10^{-1}

Abbreviations: pLOF, predicted loss of function; P_sexdiff, p-value for the significance of the difference in women and men beta values; Pval, STAAR-O p-value; Beta, effect size; SE, standard error; RR, reference/reference genotype; RA, reference/alternate genotypes; AA alternate/alternate genotypes.

Supplementary Table 8: Quality control measurements for variants included in the refined gene-based tests and single marker association results for all included variants.

[Excel file: SupplementaryTable8_WHRadjBMI.xlsx]

Supplementary Table 9: a. Summary statistics for quantitative traits from gene-based association analyses in sex-combined, women-only and male-only data. b. Summary statistics for binary traits from gene-based association analyses in sex-combined, women-only and male-only data. Details for all phenotypes and are given on Supplementary Table 12.

[Excel file: SupplementaryTable9_WHRadjBMI.xlsx]

Abbreviations: pLOF, predicted loss of function; Pval, STAAR-O p-value for phenotypic traits in Supplementary Table 9a and generalized linear model for binary traits Supplementary Table 9b; Beta, effect size; SE, standard error; Beta_LCI, lower 95% confidence interval for effect size in; Beta_UCI, upper 95% confidence interval for effect size; TG, triglyceride; HDL, high-density lipoprotein; LDL, low-density lipoprotein.

Supplementary Table 10: a. Lookup from Type 2 Diabetes Knowledge Portal for type 2 diabetes. Seven different masks were applied to filter the variants used in the association analysis: LofTee (predicted loss of function); 5/5 (predicted deleterious by 5 methods); 16/16 (predicted deleterious by 16 methods); 5/5 + LofTee LC (predicted deleterious by 5 methods, plus LofTee low confidence), 5/5 + 0/5 1% (variants predicted deleterious by 5 methods, plus variants with minor allele frequency < 1% that are not predicted to be deleterious by any of 5 methods); 5/5 + 1/5 1% (variants predicted deleterious by 5 methods, plus variants with minor allele frequency < 1% that are predicted to be deleterious by 1 of 5 methods); and 11/11 (predicted deleterious by 11 methods). Rows in bold have P-value ≤ 0.05 . Accessed from <https://t2d.hugeamp.org/> on 02/09/2021. **b. Lookup from AstraZeneca PheWAS Portal (3) for type 2 diabetes, non-insulin-dependent diabetes mellitus (Union#E11#E11) and chronic ischaemic heart disease (Union#I25#I25).** The variant categories used in collapsing models are provided in the parentheses in ‘Collapsing Model’ column. Rows in bold have P-value ≤ 0.05 . Accessed from <https://azphewas.com/> on 02/09/2021.

a.

Gene	Mask	P-value	Combined AF	Passing Variants	Singleton Variants	Standard Error	Sample Size	Odds Ratio
<i>PLIN4</i>	LofTee	0.042	0.0042	17	6	0.153	43,125	1.3641
<i>PLIN4</i>	16/16	0.042	0.0042	17	6	0.153	43,125	1.3641
<i>PLIN4</i>	11/11	0.042	0.0042	17	6	0.153	43,125	1.3641
<i>PLIN4</i>	5/5	0.907	0.0115	24	8	0.094	43,125	1.0110
<i>PLIN4</i>	5/5 + LofTee LC	0.907	0.0115	24	8	0.094	43,125	1.0110
<i>PLIN4</i>	5/5 + 1/5 1%	0.793	0.0350	174	59	0.051	43,125	1.0134
<i>PLIN4</i>	5/5 + 0/5 1%	0.653	0.0547	307	111	0.039	43,125	0.9825
<i>PLINI</i>	11/11	0.478	0.0009	11	5	0.337	43,125	0.7905
<i>PLINI</i>	5/5	0.237	0.0033	19	10	0.171	43,125	0.8178
<i>PLINI</i>	5/5 + LofTee LC	0.237	0.0033	19	10	0.171	43,125	0.8178
<i>PLINI</i>	5/5 + 1/5 1%	0.928	0.0121	87	39	0.089	43,125	0.9920
<i>PLINI</i>	5/5 + 0/5 1%	0.678	0.0153	132	56	0.079	43,125	0.9679
<i>INSR</i>	LofTee	0.017	0.0003	11	10	0.595	43,125	3.6645
<i>INSR</i>	16/16	0.015	0.0004	13	11	0.536	43,125	3.3304
<i>INSR</i>	11/11	0.229	0.0008	24	18	0.343	43,125	1.4992
<i>INSR</i>	5/5	0.836	0.0012	32	24	0.282	43,125	1.0596
<i>INSR</i>	5/5 + LofTee LC	0.836	0.0012	32	24	0.282	43,125	1.0596
<i>INSR</i>	5/5 + 1/5 1%	0.814	0.0234	212	128	0.064	43,125	0.9850

INSR	5/5 + 0/5 1%	0.803	0.0284	251	145	0.058	43,125	0.9855
ACVRIC	LofTee	0.534	0.0000	2	2	2.112	43,125	0.3845
ACVRIC	16/16	0.056	0.0001	5	5	1.654	43,125	0.1131
ACVRIC	11/11	0.084	0.0019	14	10	0.240	43,125	0.6662
ACVRIC	5/5	0.053	0.0020	15	10	0.238	43,125	0.6380
ACVRIC	5/5 + LofTee LC	0.053	0.0020	15	10	0.238	43,125	0.6380
ACVRIC	5/5 + 1/5 1%	0.152	0.0127	67	40	0.090	43,125	0.8791
ACVRIC	5/5 + 0/5 1%	0.119	0.0132	79	47	0.089	43,125	0.8717
PDE3B	LofTee	0.562	0.0010	12	9	0.316	43,125	0.8349
PDE3B	16/16	0.678	0.0010	13	10	0.311	43,125	0.8802
PDE3B	11/11	0.739	0.0013	21	17	0.280	43,125	0.9118
PDE3B	5/5	0.847	0.0020	37	27	0.222	43,125	0.9584
PDE3B	5/5 + LofTee LC	0.766	0.0020	38	28	0.221	43,125	0.9369
PDE3B	5/5 + 1/5 1%	0.770	0.0238	178	98	0.064	43,125	0.9815
PDE3B	5/5 + 0/5 1%	0.829	0.0331	263	148	0.054	43,125	1.0116

b.

Gene	Phenotype	Collapsing model (Explanation)	P value	No. participants	No. cases with QV	No. controls with QV	Odds ratio	Odds ratio LCI	Odds ratio UCI
<i>PLIN4</i>	Type 2 diabetes	Synonymous negative control (synonymous variants with MAF≤0.05%)	8.69×10 ⁻²	162,620	14	844	1.60	0.94	2.72
<i>PLIN1</i>	Type 2 diabetes	NA	NA	NA	NA	NA	NA	NA	NA
<i>INSR</i>	Type 2 diabetes	NA	NA	NA	NA	NA	NA	NA	NA
<i>ACVR1C</i>	Type 2 diabetes	Ultra-rare damaging (non-synonymous variants with MAF≤0.005%, REVEL score ≥ 0.25)	6.95×10 ⁻²	162,620	3	89	3.25	1.03	10.28
<i>PDE3B</i>	Type 2 diabetes	Non-synonymous recessive (non-synonymous variants with MAF≤1%)	9.23×10 ⁻²	162,620	3	101	2.86	0.91	9.04
<i>PLIN1</i>	Non-insulin-dependent diabetes mellitus (Union#E11#E11)	NA	NA	NA	NA	NA	NA	NA	NA
<i>PLIN4</i>	Non-insulin-dependent diabetes mellitus (Union#E11#E11)	NA	NA	NA	NA	NA	NA	NA	NA
<i>INSR</i>	Non-insulin-dependent diabetes mellitus (Union#E11#E11)	NA	NA	NA	NA	NA	NA	NA	NA
<i>ACVR1C</i>	Non-insulin-dependent diabetes mellitus (Union#E11#E11)	NA	NA	NA	NA	NA	NA	NA	NA
<i>PDE3B</i>	Non-insulin-dependent diabetes mellitus (Union#E11#E11)	Non-synonymous recessive (non-synonymous variants with MAF≤1%)	9.66×10 ⁻²	201,921	18	107	1.54	0.94	2.54
<i>PLIN4</i>	Chronic ischaemic heart disease (Union#I25#I25)	NA	NA	NA	NA	NA	NA	NA	NA
<i>PLIN1</i>	Chronic ischaemic heart disease (Union#I25#I25)	Flexible MAF, damaging non-synonymous (non-synonymous variants with MAF≤0.1%, REVEL score ≥ 0.25)	2.67×10 ⁻²	176170	48	424	0.71	0.53	0.96
		Flexible MAF, all non-synonymous (non-synonymous variants with MAF≤0.1%)	1.88×10 ⁻²	176170	179	1355	0.83	0.71	0.97
		Flexible MAF, non-synonymous, Missense Tolerance Ratio (MTR) informed (non-synonymous variants with MAF≤0.1%, MTR <25 th %ile or intergenic MTR < 50 th %ile)	9.70×10 ⁻³	176,170	88	740	0.75	0.60	0.93
		Protein truncating (protein truncating variants with MAF≤0.1%)	4.49×10⁻⁴	176,170	22	284	0.49	0.32	0.75

		Protein truncating (protein truncating variants with MAF≤5%)	4.49×10⁻⁴	176,170	22	284	0.49	0.32	0.75
		Protein truncating or rare damaging models combined (protein truncating variants with MAF≤5% and missense variants with MAF≤0.025% and REVEL score ≥ 0.25)	4.64×10 ⁻⁴	176,170	32	369	0.55	0.38	0.78
<i>PLIN1</i>	Chronic ischaemic heart disease (Union#I25#I25)	Non-synonymous recessive (non-synonymous variants with MAF≤1%)	8.51×10 ⁻²	176,170	12	129	0.59	0.32	1.06
<i>INSR</i>	Chronic ischaemic heart disease (Union#I25#I25)	Rare damaging missense (missense variants with MAF≤0.025% and REVEL score ≥ 0.25)	9.84×10 ⁻²	176,170	133	715	1.17	0.97	1.41
		Rare damaging, MTR informed (missense variants with MAF≤0.025% and REVEL score ≥ 0.25, MTR <25 th %ile or intergenic MTR < 50 th %ile)	5.06×10 ⁻²	176,170	100	506	1.25	1.00	1.54
<i>ACVR1C</i>	Chronic ischaemic heart disease (Union#I25#I25))	NA	NA	NA	NA	NA	NA	NA	NA
<i>PDE3B</i>	Chronic ischaemic heart disease (Union#I25#I25)	Rare damaging, MTR informed (missense variants with MAF≤0.025% and REVEL score ≥ 0.25, MTR <25 th %ile or intergenic MTR < 50 th %ile)	4.98×10 ⁻²	176,170	38	335	0.71	0.51	1.00
		Non-synonymous recessive (non-synonymous variants with MAF≤1%)	8.57×10 ⁻²	176,170	8	96	0.52	0.25	1.08

Abbreviations: QV, qualifying variant; LCI, lower 95% confidence interval; UCI, upper 95% confidence interval; NA, not available.

Supplementary Table 11: Leave one out analysis results for the most significant single variant in significant genes.

Category	Gene	Variant	chr	pos	Major Allele	Minor Allele	Consequence	MAF	Gene-based p-value	Gene-based p value after dropping the variant
pLoF	<i>PLIN4</i> p.Q372X	rs201581703	19	4512804	G	A	Stop gained	0.158%	5.86×10^{-7}	1.79×10^{-4}
pLoF	<i>PLIN1</i> p.T338DfsX51	rs750619494	15	89667122	CTTCTGC AGGGT	C	Frameshift variant	0.029%	9.82×10^{-9}	9.29×10^{-4}
pLoF	<i>INSR</i> p.525RX	rs1599937180	19	7168005	G	A	Stop gained	0.001%	6.21×10^{-7}	2.61×10^{-4}
Moderate	<i>ACVR1C</i> p.I195T	rs56188432	2	15755035 3	A	G	Missense variant	0.208%	4.57×10^{-7}	0.026
pLoF+ Moderate	<i>ACVR1C</i> p.I195T	rs56188432	2	15755035 3	A	G	Missense variant	0.208%	1.68×10^{-7}	0.011
pLoF	<i>PDE3B</i> p.R783X	rs150090666	11	14843853	C	T	Stop gained	0.095%	1.41×10^{-6}	0.493

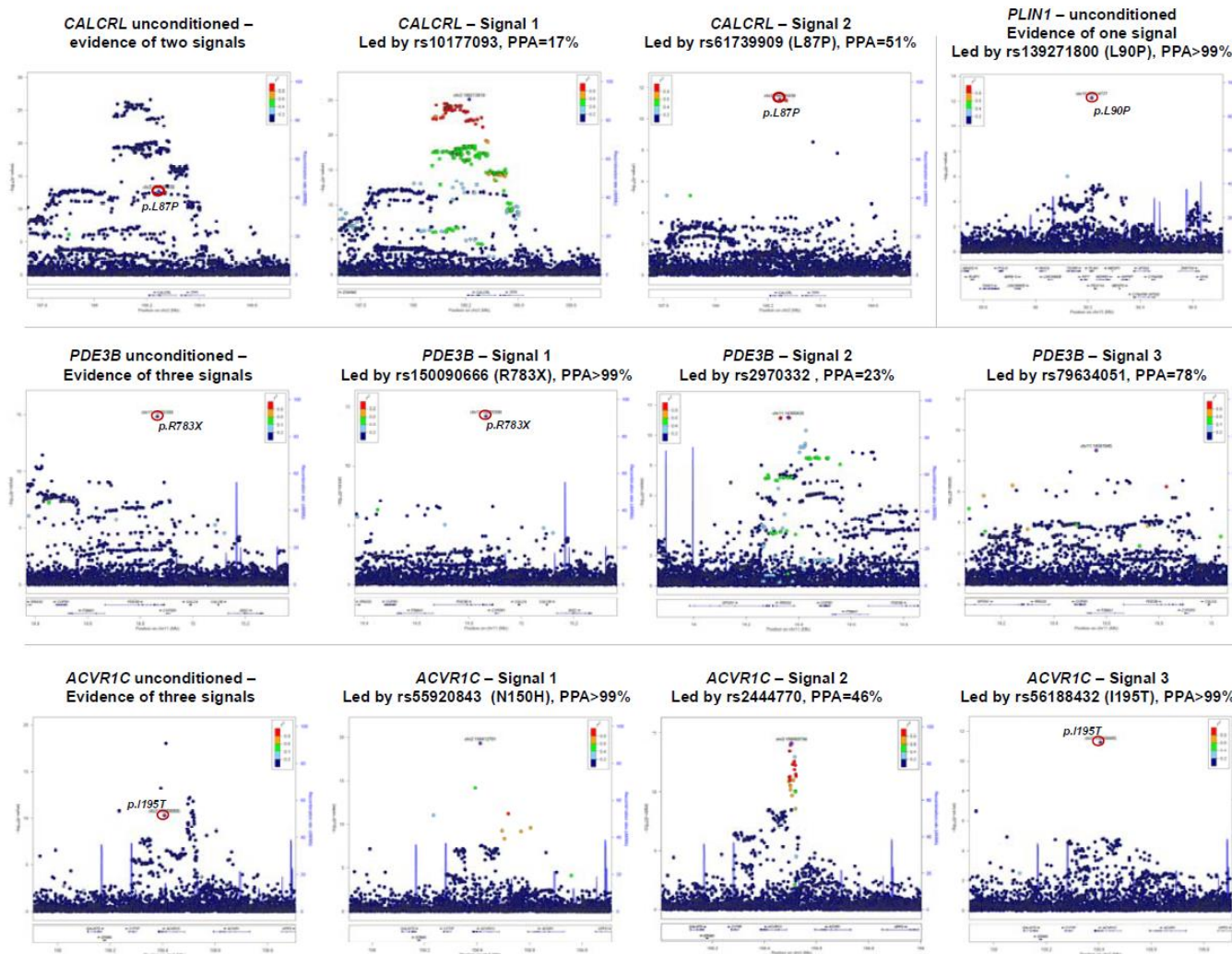
Abbreviations: pLOF, predicted loss of function; chr, chromosome; pos, position (b38); MAF, minor allele frequency; Pval, STAAR-O p-value; Beta, effect size; SE, standard error; RR, reference/reference genotype; RA, reference/alternate genotypes; AA alternate/alternate genotypes.

Supplementary Table 12. Phenotypes used for phenotypic associations in UK Biobank. Sex (for sex-combined analyses), sequencing batch (50K vs. 150K), genotyping array, and 10 genetic principal components were included as covariates in association analyses.

Outcome	Cases, N	Non-cases (for case-control studies) or participants (for continuous traits studies) in sub-study, N	Adjustments for the phenotype
BMI	NA	184,291	RB-INV transformed
Gynoid fat	NA	178,143	logn transformed, adjusted for age and logn total body fat, RB-INV of residuals within each sex separately
Android fat	NA	178,143	logn transformed, adjusted for age and logn total body fat, RB-INV of residuals within each sex separately
Leg fat	NA	178,143	logn transformed, adjusted for age and logn total body fat, RB-INV of residuals within each sex separately
Arm fat	NA	178,143	logn transformed, adjusted for age and logn total body fat, RB-INV of residuals within each sex separately
Trunk fat	NA	178,143	logn transformed, adjusted for age and logn total body fat, RB-INV of residuals within each sex separately
HbA1c	NA	175,778	RB-INV transform within aliquots, excluded prevalent T2D cases.
HDL cholesterol	NA	161,239	RB-INV transform within aliquots
LDL cholesterol	NA	146,020	RB-INV transform within aliquots, statin users were excluded
Triglycerides (TG)	NA	175,271	ln transformed, RB-INV transform within aliquots
TG/HDL ratio	NA	161,102	RB-INV transform within aliquots
Type 2 Diabetes	12875	171,462	According to the previously published UKBB probable T2D algorithm (27631769) based on baseline self-reported diabetes or medications, in addition to evidence from electronic health records (Hospital Episode Statistics or Death Registration) consistent with T2D (International Statistical Classification of Diseases and Related Health Problems Tenth Revision code E11)
Coronary Heart Disease	11821	172,516	Based on CALIBER working group's definition based on primary and secondary care records in UK Biobank

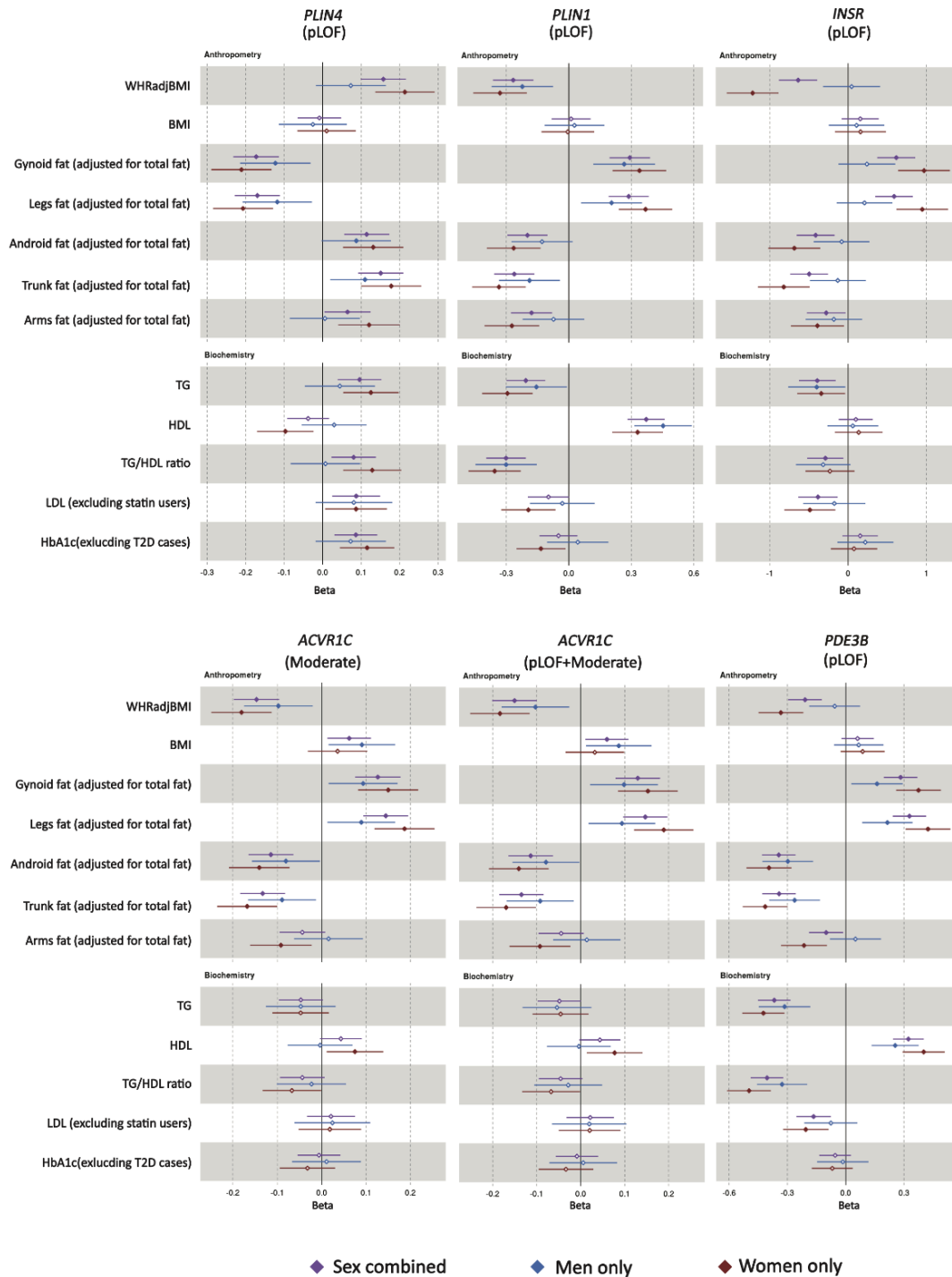
Abbreviations: BMI, body mass index; HDL high-density lipoproteins; LDL low-density lipoproteins; RB-INV, rank-based inverse normal transformation; NA, not available.

Supplementary Figure 1: Regional association plots of the overall and statistically-decomposed signals at the *CALCRL*, *PLIN1*, *PDE3B* and *ACVR1C* genes. Plots were drawn using LocusZoom (4). Joint meta-analysis models using GCTA (1) were used at each locus to assess how many independent signals were present. Then, at each locus each signal was statistically-decomposed from others by estimating associations of all variants in the region adjusted for all other index variants at the region. Fine-mapping of each signal was performed using a Bayesian approach (5).

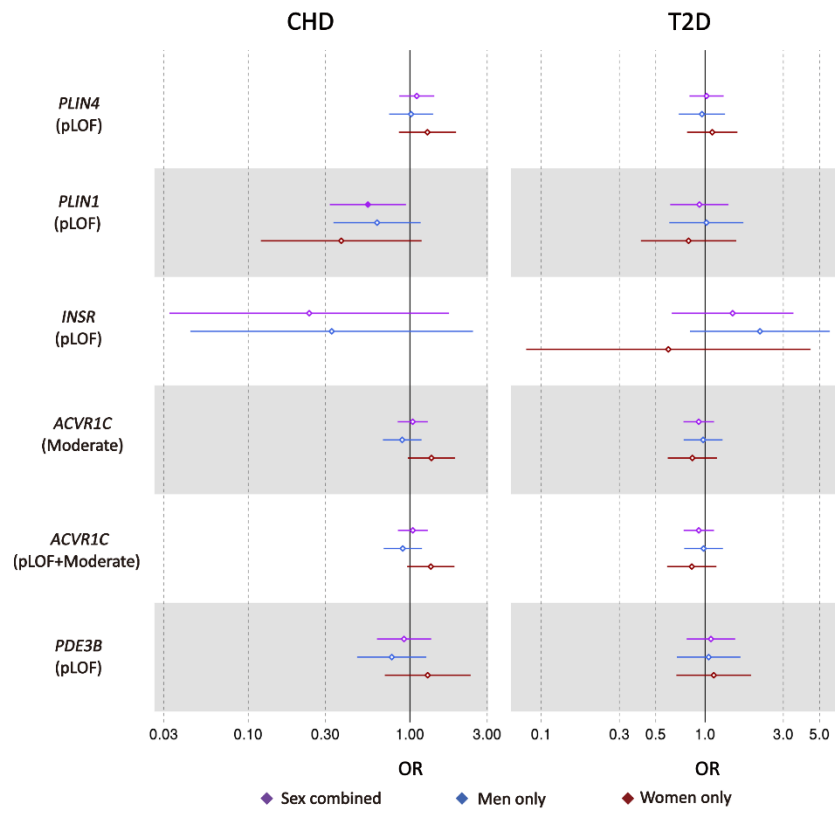


Supplementary Figure 2: Association of the significant genes with other body fat distribution or cardiometabolic trait related phenotypes in UK Biobank for (a) continuous phenotypes and (b) binary phenotypes. There was no rare predicted loss of function variant carriers for *INSR* in coronary heart disease (CHD) cases in women-only analyses. Abbreviations: pLoF, predicted loss of function; OR, odds ratio; WHRadjBMI; waist-to-hip ratio adjusted for body mass index; BMI, body mass index; TG, triglycerides; HD; high density lipoprotein, LDL low-density lipoprotein; TG/HDL, triglyceride to high density lipoprotein ratio; T2D, type 2 diabetes; CHD, coronary heart disease.

a.



b.



Supplementary Note 1: Genomic context analyses at the *PLINI*, *ACVR1C*, *PDE3B* and *CALCRL* loci.

Fine-mapping analyses provided strong statistical evidence for the causal association of rare nonsynonymous variants of *CALCRL*, *PLINI*, *PDE3B* and *ACVR1C*.

At *PLINI*, there was evidence of only one signal led by the rare p.L90P variant (rs139271800; Supplementary Figure 1), which was the only variant in the 99% credible set (PPA>99%; Supplementary Table 3).

At *ACVR1C*, there was evidence of three distinct signals (Supplementary Figure 1, Supplementary Table 3). The rare p.I195T variant led one of the secondary signals at this region and was the only variant in the 99% credible set (PPA>99%; Supplementary Table 3). In addition, the primary signal at this region was led by a low-frequency missense variant in *ACVR1C* (rs55920843, p.N150H), which also had the highest posterior probability in fine-mapping of this signal (PPA>99%; Table 1). Hence, fine-mapping of conditionally-independent signals at this locus converges on *ACVR1C* as causal gene for body fat distribution and p.I195T and p.N150H as causal variants for the respective association peaks.

At *PDE3B*, there was evidence of three signals, the strongest of which was led by the rs150090666 p.R783X nonsense variant in *PDE3B*, which was the only variant in the 99% credible set (PPA>99%; Supplementary Figure 1, Supplementary Table 3).

At *CALCRL*, there was evidence of two conditionally-independent signals (Supplementary Figure 1, Supplementary Table 3), led by the rs10177093 common variant and by the rare p.L87P variant, respectively. Fine-mapping at the latter signal yielded a 99% credible set including only two variants, rs61739909 (*CALCRL* p.L87P, posterior probability of casual association [PPA]=51%) and rs180960888 (intronic to *CALCRL*, PPA=48.5%). Hence, p.L87P is the most likely causal variant and *CALCRL* the most likely causal gene for this signal.

Supplementary Note 2: Genomic context analyses at the *ABHD15*, *PYGM*, *PLCB3* and *FNIP1* loci.

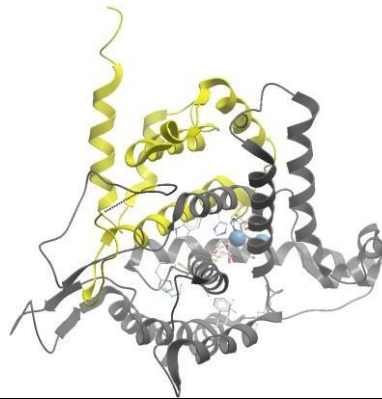
In the main analysis, we found associations of rare nonsynonymous variants in *ABHD15* and *PYGM* for which genomic context analyses were not consistent with a causal association. At *ABHD15*, conditional analyses revealed two distinct association signals tagged by the rs62070804 and rs561089333 index-variants respectively (Supplementary Table 4). The rare nonsynonymous rs141385558 p.G147D variant was not among these index variants and its association was greatly attenuated after adjusting for the two independent index variants ($p_{conditional}=0.00019$; Supplementary Table 1). At *PYGM*, there was a complex association pattern with evidence of up to 12 distinct signals (Supplementary Table 4). The rare nonsense rs116987552 p.R50X variant was not among these 12 index variants and its association was greatly attenuated after adjusting for these 12 index variants ($p_{conditional}=0.00037$; Supplementary Table 1). In the secondary analyses, we found associations of rare nonsynonymous variants in *PLCB3* (both in experiment-level p-value and sex-specific analyses) and *FNIP1* (sex-specific analyses) for which genomic context analyses were not consistent with a causal association. At *PLCB3*, there was evidence of up to ten independent signals (Supplementary Table 4) but the p.V806I variant was not among those and adjusting for the conditionally-independent index variants greatly attenuated its association ($p_{conditional}>0.10$; Supplementary Table 1). At *FNIP1* there was evidence of only one signal but the p.R518Q missense variant was not the lead variant (Supplementary Table 4). Adjusting for the lead variant attenuated the signal ($p_{conditional}=3.8\times 10^{-7}$; Supplementary Table 1) and the variant had low posterior probability in the fine-mapping analysis (PPA=8.7%).

Supplementary Note 3: Predictions regarding the variants identified through single marker analysis.

Gene, allele Gene product	Information on gene function, structural modelling and biological insights of associations reported in this study																																																																																																																																																																																																																																																																																														
<p><i>PLIN1</i> p.L90P Perilipin 1</p>	<p>Perilipin 1 is a constitutive lipid droplet-associated protein predominantly expressed in adipocytes, where it is necessary for optimal triglyceride storage and for the precisely regulated release of fatty acids from the droplet (6). Perilipin 1 has a well-established role as a negative regulator of intracellular lipolysis (7, 8). Rare loss-of-function mutations in <i>PLIN1</i> cause autosomal dominant forms of partial lipodystrophy with lack of gluteo-femoral and leg fat, insulin resistance, dyslipidemia and type 2 diabetes (9). Leucine 90 is conserved in <i>Mammalia</i> and <i>Sauria</i> and replaced conservatively in lower species (<i>Inset Figure 1</i>). It lies at the N-terminal edge of the highly-conserved PAT domain responsible for the interaction with hormone sensitive lipase, the enzyme that catalyzes intracellular diglyceride hydrolysis (10). Although the structure of this region is unknown, it is predicted to be highly helical and the substitution of leucine with proline at position 90 is predicted to break the helix, introducing a sharp kink (<i>Inset Figure 2</i>). Thus, p.L90P, which is associated with lower waist- to-hip ratio, higher overall adiposity, and lipid levels in our human genetic studies, may affect intracellular lipolysis by impacting on perilipin 1 interaction with hormone sensitive lipase. Our results show that nonsynonymous variation in this gene influences fat distribution and lipid levels in the general population, adding to the notion of shared genetic mechanisms between severe and subtle forms of human lipodystrophy (11).</p> <div style="text-align: center;"> <table border="1" style="margin: auto;"> <tr> <td>Homo_sapiens</td> <td>77</td> <td>V</td><td>R</td><td>R</td><td>L</td><td>S</td> <td>T</td><td>Q</td><td>F</td><td>T</td><td>A</td><td>A</td><td>N</td><td>E</td> <td>L</td><td>A</td><td>C</td><td>R</td><td>G</td><td>L</td><td>D</td><td>H</td><td>L</td><td>E</td> <td>99</td> </tr> <tr> <td>Mus_musculus</td> <td>77</td> <td>V</td><td>R</td><td>R</td><td>L</td><td>S</td> <td>T</td><td>Q</td><td>F</td><td>T</td><td>A</td><td>A</td><td>N</td><td>E</td> <td>L</td><td>A</td><td>C</td><td>R</td><td>G</td><td>L</td><td>D</td><td>H</td><td>L</td><td>E</td> <td>99</td> </tr> <tr> <td>Monodelphis_domestica</td> <td>77</td> <td>V</td><td>R</td><td>R</td><td>L</td><td>S</td> <td>T</td><td>Q</td><td>F</td><td>T</td><td>A</td><td>A</td><td>N</td><td>E</td> <td>L</td><td>A</td><td>C</td><td>R</td><td>G</td><td>L</td><td>D</td><td>H</td><td>L</td><td>E</td> <td>99</td> </tr> <tr> <td>Ornithorhynchus_anatinus</td> <td>92</td> <td>V</td><td>R</td><td>K</td><td>L</td><td>E</td> <td>P</td><td>Q</td><td>F</td><td>T</td><td>A</td><td>A</td><td>N</td><td>E</td> <td>L</td><td>A</td><td>C</td><td>R</td><td>G</td><td>L</td><td>D</td><td>H</td><td>L</td><td>E</td> <td>114</td> </tr> <tr> <td>Gallus_gallus</td> <td>75</td> <td>V</td><td>R</td><td>R</td><td>L</td><td>E</td> <td>P</td><td>Q</td><td>F</td><td>S</td><td>M</td><td>A</td><td>N</td><td>T</td> <td>L</td><td>A</td><td>C</td><td>R</td><td>G</td><td>L</td><td>D</td><td>H</td><td>L</td><td>E</td> <td>97</td> </tr> <tr> <td>Xenopus_tropicalis</td> <td>91</td> <td>V</td><td>K</td><td>T</td><td>F</td><td>E</td> <td>H</td><td>Q</td><td>I</td><td>S</td><td>A</td><td>A</td><td>N</td><td>E</td> <td>I</td><td>A</td><td>C</td><td>K</td><td>G</td><td>M</td><td>D</td><td>R</td><td>L</td><td>E</td> <td>113</td> </tr> <tr> <td>Latimeria_chalumnae</td> <td>75</td> <td>L</td><td>Q</td><td>R</td><td>L</td><td>E</td> <td>P</td><td>Q</td><td>I</td><td>T</td><td>A</td><td>A</td><td>D</td><td>N</td> <td>I</td><td>A</td><td>C</td><td>I</td><td>G</td><td>L</td><td>D</td><td>H</td><td>L</td><td>E</td> <td>97</td> </tr> <tr> <td>Danio_rerio</td> <td>74</td> <td>L</td><td>H</td><td>V</td><td>L</td><td>Q</td> <td>P</td><td>Q</td><td>L</td><td>V</td><td>A</td><td>A</td><td>N</td><td>S</td> <td>M</td><td>A</td><td>C</td><td>K</td><td>G</td><td>L</td><td>D</td><td>R</td><td>L</td><td>E</td> <td>96</td> </tr> <tr> <td>Plin2</td> <td>69</td> <td>I</td><td>Q</td><td>K</td><td>L</td><td>E</td> <td>P</td><td>Q</td><td>I</td><td>A</td><td>V</td><td>A</td><td>N</td><td>T</td> <td>Y</td><td>A</td><td>C</td><td>K</td><td>G</td><td>L</td><td>D</td><td>R</td><td>I</td><td>E</td> <td>91</td> </tr> <tr> <td>Plin3</td> <td>82</td> <td>L</td><td>S</td><td>K</td><td>L</td><td>E</td> <td>P</td><td>Q</td><td>I</td><td>A</td><td>S</td><td>A</td><td>S</td><td>E</td> <td>Y</td><td>A</td><td>H</td><td>R</td><td>G</td><td>L</td><td>D</td><td>K</td><td>L</td><td>E</td> <td>104</td> </tr> <tr> <td>Plin5</td> <td>79</td> <td>L</td><td>E</td><td>H</td><td>L</td><td>Q</td> <td>P</td><td>Q</td><td>L</td><td>A</td><td>T</td><td>M</td><td>N</td><td>S</td> <td>L</td><td>A</td><td>C</td><td>R</td><td>G</td><td>L</td><td>D</td><td>K</td><td>L</td><td>E</td> <td>101</td> </tr> </table> </div> <p><i>Inset Figure 1.</i> Sequence alignment of perilipin 1 segments from representative species and human perilipin 2, 3 and 5. Perilipin 4 is not included due to divergence and multiplication of its N-terminus. The structure of the segment is modelled in <i>Inset Figure 2</i>. Arrows indicate the mutated L90 (red) and phosphorylated S81 (black).</p> <div style="text-align: center;"> </div> <p><i>Inset Figure 2.</i> Comparison of models of the native (blue) and mutated (green) fragment of perilipin 1 including amino acids 77 through 99. Built on the helical fragment of Protein Data Bank structure 4BJM/205-228 and superposed for the minimal root-mean-square deviation of the backbone (red) between L90 and P90. Their side chains are displayed together with S81 in ball and stick representation.</p>	Homo_sapiens	77	V	R	R	L	S	T	Q	F	T	A	A	N	E	L	A	C	R	G	L	D	H	L	E	99	Mus_musculus	77	V	R	R	L	S	T	Q	F	T	A	A	N	E	L	A	C	R	G	L	D	H	L	E	99	Monodelphis_domestica	77	V	R	R	L	S	T	Q	F	T	A	A	N	E	L	A	C	R	G	L	D	H	L	E	99	Ornithorhynchus_anatinus	92	V	R	K	L	E	P	Q	F	T	A	A	N	E	L	A	C	R	G	L	D	H	L	E	114	Gallus_gallus	75	V	R	R	L	E	P	Q	F	S	M	A	N	T	L	A	C	R	G	L	D	H	L	E	97	Xenopus_tropicalis	91	V	K	T	F	E	H	Q	I	S	A	A	N	E	I	A	C	K	G	M	D	R	L	E	113	Latimeria_chalumnae	75	L	Q	R	L	E	P	Q	I	T	A	A	D	N	I	A	C	I	G	L	D	H	L	E	97	Danio_rerio	74	L	H	V	L	Q	P	Q	L	V	A	A	N	S	M	A	C	K	G	L	D	R	L	E	96	Plin2	69	I	Q	K	L	E	P	Q	I	A	V	A	N	T	Y	A	C	K	G	L	D	R	I	E	91	Plin3	82	L	S	K	L	E	P	Q	I	A	S	A	S	E	Y	A	H	R	G	L	D	K	L	E	104	Plin5	79	L	E	H	L	Q	P	Q	L	A	T	M	N	S	L	A	C	R	G	L	D	K	L	E	101
Homo_sapiens	77	V	R	R	L	S	T	Q	F	T	A	A	N	E	L	A	C	R	G	L	D	H	L	E	99																																																																																																																																																																																																																																																																						
Mus_musculus	77	V	R	R	L	S	T	Q	F	T	A	A	N	E	L	A	C	R	G	L	D	H	L	E	99																																																																																																																																																																																																																																																																						
Monodelphis_domestica	77	V	R	R	L	S	T	Q	F	T	A	A	N	E	L	A	C	R	G	L	D	H	L	E	99																																																																																																																																																																																																																																																																						
Ornithorhynchus_anatinus	92	V	R	K	L	E	P	Q	F	T	A	A	N	E	L	A	C	R	G	L	D	H	L	E	114																																																																																																																																																																																																																																																																						
Gallus_gallus	75	V	R	R	L	E	P	Q	F	S	M	A	N	T	L	A	C	R	G	L	D	H	L	E	97																																																																																																																																																																																																																																																																						
Xenopus_tropicalis	91	V	K	T	F	E	H	Q	I	S	A	A	N	E	I	A	C	K	G	M	D	R	L	E	113																																																																																																																																																																																																																																																																						
Latimeria_chalumnae	75	L	Q	R	L	E	P	Q	I	T	A	A	D	N	I	A	C	I	G	L	D	H	L	E	97																																																																																																																																																																																																																																																																						
Danio_rerio	74	L	H	V	L	Q	P	Q	L	V	A	A	N	S	M	A	C	K	G	L	D	R	L	E	96																																																																																																																																																																																																																																																																						
Plin2	69	I	Q	K	L	E	P	Q	I	A	V	A	N	T	Y	A	C	K	G	L	D	R	I	E	91																																																																																																																																																																																																																																																																						
Plin3	82	L	S	K	L	E	P	Q	I	A	S	A	S	E	Y	A	H	R	G	L	D	K	L	E	104																																																																																																																																																																																																																																																																						
Plin5	79	L	E	H	L	Q	P	Q	L	A	T	M	N	S	L	A	C	R	G	L	D	K	L	E	101																																																																																																																																																																																																																																																																						

PDE3B p.R783X
Phosphodiesterase 3B

Phosphodiesterase 3B is a membrane bound phosphodiesterase highly expressed in adipocytes, where it has been implicated in terminating intracellular lipolysis in response to insulin by degrading cyclic adenosine monophosphate (12). Phosphodiesterase 3B null mice manifest enhanced intracellular lipolysis, lower fat mass but higher insulin resistance (13). The premature stop codon generated by p.R783X falls within the proximal half of the catalytic domain of phosphodiesterase 3B, removing most of its Mg^{2+} binding site (*Inset Figure 3*). Hence, this rare null variant, associated in our human genetic studies with lower waist-to-hip ratio, higher levels of peripheral adiposity and lower blood pressure and triglycerides is expected to result in a loss of catalytic function of phosphodiesterase 3B. If the protein is expressed, it could be embedded in the membrane through its intact N-terminal 6 membrane spanning domains and impair the phosphodiesterase 3B signalling complex (14) in a dominant-negative manner. Therefore, our data provide evidence of causal link between the loss of phosphodiesterase 3B function and greater peripheral fat, more favourable fat distribution and lower blood pressure

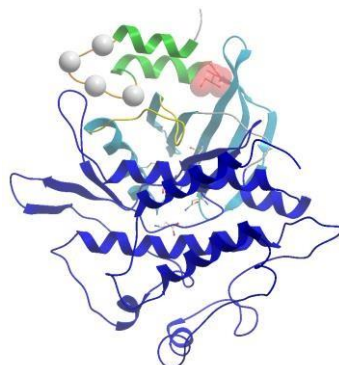


and atherogenic lipids in humans. The effect size of this null allele on waist-to-hip ratio is over 6-fold greater than that of the strongest alleles found in GWAS of common variants (15).

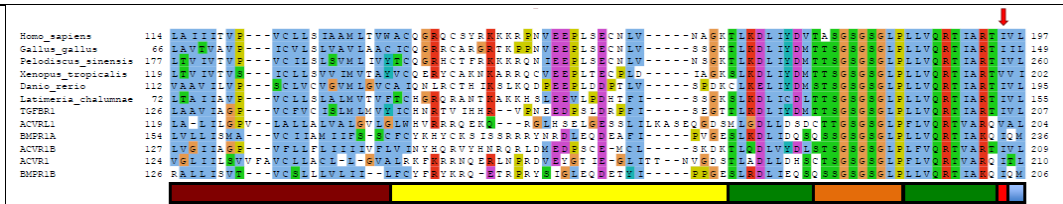
Inset Figure 3. Structure of the catalytic domain of PDE3B (Protein Data Bank coordinates 1SO2 (16)) with an inhibitor in the active site (Protein Data Bank coordinates 1ISO2((17))). The mutation R783X removes the protein part highlighted in grey. The N-terminus at the top of the figure is preceded by a 6 trans membrane helical domain. Inhibitor and active site residues are in ball and stick representation and the two blue balls indicate Mg^{2+} ions.

ACVR1C p.I195T
Activin A Receptor Type 1C

The Activin A Receptor Type 1C is type I member of the family of transforming growth factor beta receptors transmitting signals from extracellular ligands to nuclear transcription. *ACVR1C* downregulates the key fat storage and glucose metabolism regulator peroxisome proliferator-activated receptor gamma (18). *ACVR1C* inhibits β -adrenergic signalling, mitochondrial biogenesis, lipid oxidation, and intracellular lipolysis in adipocytes (18). The *Inset Figure 4* shows a structural model of the intracellular part of *ACVR1C*. It can be seen that I195 forms a hinge between the N-terminal regulatory GS-domain and the kinase. Its side chain is tightly packed against both the kinase and the GS-domain. The serine/threonine epitope in the phosphorylation loop of the GS-domain is wedged in the active site between the kinase N- and C-lobes blocking access to the active site. Upon activation (phosphorylation), the GS-domain liberates the active site and interacts with its SMAD protein substrates. I195 is expected to be involved in any mutual GS- and kinase domain movement. Its side chain is buried in a hydrophobic environment and the change from aliphatic to polar residue should be significant. I195 is strictly conserved in all orthologues and in most metazoan paralogues including the 6 other human ones (*Inset Figure 5*). The rare replacements by different aliphatic amino acids (L, V) are very conservative. The mutation may influence kinase regulation as well as interaction with SMADs.



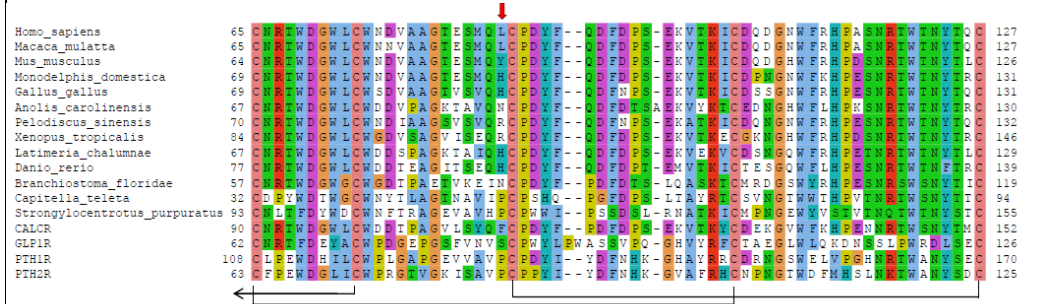
Inset Figure 4. Model of *ACVR1C* stabilized in its inactive conformation built according to the structure of TGFBR1 (Protein Data Bank coordinates 1B6C (19)). The N-terminus pointing to the membrane is on the top. The kinase domain is colored in blue, its N- and C-lobes distinguished in light and dark with the catalytic side-chains displayed in ball and stick and the activation loop in yellow. The regulatory GS-domain is in green with the phosphorylation epitope in orange and the alpha carbons of the residues to be phosphorylated upon activation highlighted by balls. The mutated L195 in ball and stick and space filling representation is in red.



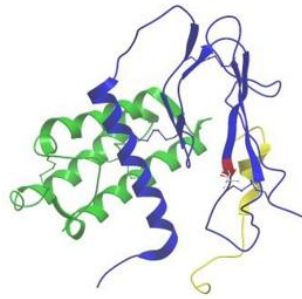
Inset Figure 5. Alignment of AVCR1C sequence segments from representative species and the human paralogues from TGF-beta family. The segment covers the transmembrane domain (brown), linker (yellow), GS-domain (green) with the phosphorylation loop (orange) followed by a hinge (red) and the first beta-strand of the kinase (blue). The latter four elements can be seen in 3D in *Inset Figure 4* using the same color coding. Arrow indicate the mutated I195.

CALCRL p.L87P
Calcitonin receptor-like

Calcitonin receptor-like receptor is a G-protein coupled receptor which requires association with one of the receptor activity-modifying proteins 1-3 (RAMP1-3) for ligand binding and receptor activation (20). When associated with RAMP1, it serves as a receptor for calcitonin gene-related peptide (CGRP), whereas when associated with RAMP2-3 it functions as a receptor for adrenomedullin which is most widely recognized as a vasoactive peptide (21, 22). Mouse knockouts of adrenomedullin (23) and CALCRL (24) are embryonic lethal. However, adrenomedullin, CALCRL and RAMP2-3 are all expressed in human adipocytes where adrenomedullin has been shown to stimulate intracellular lipolysis (25). Leucine 87 is not a conserved residue and is replaced by proline in several species (*Inset Figure 6*). The mutation is located at the tip of a strand in a beta-hairpin next to C88 and C127, both of which are strictly conserved (*Inset Figures 6-7*). The existence of the neighboring disulfide cross-link which is strictly conserved indicates that the orientation of the hairpin is important and it is indeed in close contact with RAMP2. The mutation may partially destabilize the beta-sheet, leading to a slight readjustment of the hairpin, and its interaction with adrenomedullin. The effect on ligand binding will however be indirect and probably mild in the complex with RAMP2 and adrenomedullin. However, the effect might be stronger when the receptor forms a complex with RAMP1 or 3 and interacts with different ligands. The association of p.L87P with lower waist-to-hip ratio coupled with the high expression of the CALCRL gene in adipose tissue point to a possible role in adipocyte biology of this G-protein coupled receptor.



Inset Figure 6. Sequence alignment of CALCRL segments from representative species and the closest human homologues. The disulfide bonds are indicated by black connectors and the mutated L87 by a red arrow. The fragment covers the beta-barrel in *Inset Figure 7*.



modelling.

Inset Figure 7. Structure of the extracellular portion of the complex between CALCRL (blue), RAMP2 (yellow) and adrenomedullin (green). Extensions of the C-terminus of CALCRL and the N-terminus of RAMP2 (not shown in this model) constitute the trans-membrane and intracellular domains of CALCRL and RAMP2. The position of L87 is in red and its side-chain in ball and stick representation. The side chains of the conserved structure stabilizing cysteines are also shown. Protein Data Bank coordinates 4RWF (26) were used for

REFERENCES

1. Yang J, Lee SH, Goddard ME, Visscher PM. GCTA: a tool for genome-wide complex trait analysis. *Am J Hum Genet.* 2011;88(1):76-82.
2. Li X, Li Z, Zhou H, Gaynor SM, Liu Y, Chen H, et al. Dynamic incorporation of multiple in silico functional annotations empowers rare variant association analysis of large whole-genome sequencing studies at scale. *Nat Genet.* 2020;52(9):969-83.
3. Wang Q, Dhindsa RS, Carss K, Harper AR, Nag A, Tachmazidou I, et al. Rare variant contribution to human disease in 281,104 UK Biobank exomes. *Nature.* 2021.
4. Pruim RJ, Welch RP, Sanna S, Teslovich TM, Chines PS, Gliedt TP, et al. LocusZoom: regional visualization of genome-wide association scan results. *Bioinformatics.* 2010;26(18):2336-7.
5. Maller JB, McVean G, Byrnes J, Vukcevic D, Palin K, Su Z, et al. Bayesian refinement of association signals for 14 loci in 3 common diseases. *Nat Genet.* 2012;44(12):1294-301.
6. Brasaemle DL, Subramanian V, Garcia A, Marcinkiewicz A, Rothenberg A. Perilipin A and the control of triacylglycerol metabolism. *Mol Cell Biochem.* 2009;326(1-2):15-21.
7. Granneman JG, Moore HP, Krishnamoorthy R, Rathod M. Perilipin controls lipolysis by regulating the interactions of AB-hydrolase containing 5 (Abhd5) and adipose triglyceride lipase (Atgl). *J Biol Chem.* 2009;284(50):34538-44.
8. Gandotra S, Lim K, Grousse A, Saudek V, O'Rahilly S, Savage DB. Human frame shift mutations affecting the carboxyl terminus of perilipin increase lipolysis by failing to sequester the adipose triglyceride lipase (ATGL) coactivator AB-hydrolase-containing 5 (ABHD5). *J Biol Chem.* 2011;286(40):34998-5006.
9. Gandotra S, Le Dour C, Bottomley W, Cervera P, Giral P, Reznik Y, et al. Perilipin deficiency and autosomal dominant partial lipodystrophy. *N Engl J Med.* 2011;364(8):740-8.
10. Sztalryd C, Brasaemle DL. The perilipin family of lipid droplet proteins: Gatekeepers of intracellular lipolysis. *Biochim Biophys Acta Mol Cell Biol Lipids.* 2017;1862(10 Pt B):1221-32.
11. Lotta LA, Gulati P, Day FR, Payne F, Ongen H, van de Bunt M, et al. Integrative genomic analysis implicates limited peripheral adipose storage capacity in the pathogenesis of human insulin resistance. *Nat Genet.* 2017;49(1):17-26.
12. DiPilato LM, Ahmad F, Harms M, Seale P, Manganiello V, Birnbaum MJ. The Role of PDE3B Phosphorylation in the Inhibition of Lipolysis by Insulin. *Mol Cell Biol.* 2015;35(16):2752-60.
13. Degerman E, Ahmad F, Chung YW, Guirguis E, Omar B, Stenson L, et al. From PDE3B to the regulation of energy homeostasis. *Curr Opin Pharmacol.* 2011;11(6):676-82.
14. Wilson LS, Baillie GS, Pritchard LM, Umana B, Terrin A, Zaccolo M, et al. A phosphodiesterase 3B-based signaling complex integrates exchange protein activated by cAMP 1 and phosphatidylinositol 3-kinase signals in human arterial endothelial cells. *J Biol Chem.* 2011;286(18):16285-96.

15. Shungin D, Winkler TW, Croteau-Chonka DC, Ferreira T, Locke AE, Mägi R, et al. New genetic loci link adipose and insulin biology to body fat distribution. *Nature*. 2015;518(7538):187-96.
16. Scapin G, Patel SB, Chung C, Varnerin JP, Edmondson SD, Mastracchio A, et al. Crystal structure of human phosphodiesterase 3B: atomic basis for substrate and inhibitor specificity. *Biochemistry*. 2004;43(20):6091-100.
17. ter Haar E, Koth CM, Abdul-Manan N, Swenson L, Coll JT, Lippke JA, et al. Crystal structure of the ectodomain complex of the CGRP receptor, a class-B GPCR, reveals the site of drug antagonism. *Structure*. 2010;18(9):1083-93.
18. Yogosawa S, Mizutani S, Ogawa Y, Izumi T. Activin receptor-like kinase 7 suppresses lipolysis to accumulate fat in obesity through downregulation of peroxisome proliferator-activated receptor γ and C/EBP α . *Diabetes*. 2013;62(1):115-23.
19. Huse M, Chen YG, Massagué J, Kuriyan J. Crystal structure of the cytoplasmic domain of the type I TGF beta receptor in complex with FKBP12. *Cell*. 1999;96(3):425-36.
20. Watkins HA, Chakravarthy M, Abhayawardana RS, Gingell JJ, Garelja M, Pardamwar M, et al. Receptor Activity-modifying Proteins 2 and 3 Generate Adrenomedullin Receptor Subtypes with Distinct Molecular Properties. *J Biol Chem*. 2016;291(22):11657-75.
21. Mistrova E, Wiegand S, Saviglerova J, Pfeil U, Kuncova J, Slavikova J, et al. Adrenomedullin and the calcitonin receptor-like receptor system mRNA expressions in the rat heart and sensory ganglia in experimentally-induced long-term diabetes. *Gen Physiol Biophys*. 2014;33(2):215-25.
22. Watkins HA, Walker CS, Ly KN, Bailey RJ, Barwell J, Poyner DR, et al. Receptor activity-modifying protein-dependent effects of mutations in the calcitonin receptor-like receptor: implications for adrenomedullin and calcitonin gene-related peptide pharmacology. *Br J Pharmacol*. 2014;171(3):772-88.
23. Caron KM, Smithies O. Extreme hydrops fetalis and cardiovascular abnormalities in mice lacking a functional Adrenomedullin gene. *Proc Natl Acad Sci U S A*. 2001;98(2):615-9.
24. Dackor RT, Fritz-Six K, Dunworth WP, Gibbons CL, Smithies O, Caron KM. Hydrops fetalis, cardiovascular defects, and embryonic lethality in mice lacking the calcitonin receptor-like receptor gene. *Mol Cell Biol*. 2006;26(7):2511-8.
25. Dong Y, Betancourt A, Belfort M, Yallampalli C. Targeting Adrenomedullin to Improve Lipid Homeostasis in Diabetic Pregnancies. *J Clin Endocrinol Metab*. 2017;102(9):3425-36.
26. Booe JM, Walker CS, Barwell J, Kuteyi G, Simms J, Jamaluddin MA, et al. Structural Basis for Receptor Activity-Modifying Protein-Dependent Selective Peptide Recognition by a G Protein-Coupled Receptor. *Mol Cell*. 2015;58(6):1040-52.